Journal of Hepatocellular Carcinoma

Dovepress
Taylor & Francis Group

Open Access Full Text Article

ORIGINAL RESEARCH

Preoperative Prediction of a Rare and Highly Aggressive Subtype of Hepatocellular Carcinoma Based on Multimodal Imaging and Clinical Indicators

Keke Chen[1,*], Yuli Zhu[1,*], Han Liu[2,*], Minying Deng[3], Wentao Kong[4], Wenping Wang[1]

[1]Department of Ultrasound, Zhongshan Hospital, Fudan University, Shanghai, 200032, People's Republic of China; [2]Department of Ultrasound, Huashan Hospital, Fudan University, Shanghai, 200040, People's Republic of China; [3]Department of Pathology, Zhongshan Hospital, Fudan University, Shanghai, 200032, People's Republic of China; [4]Department of Ultrasound, Nanjing Drum Tower Hospital, Affiliated Hospital of Medical School, Nanjing University, Nanjing, 210008, People's Republic of China

*These authors contributed equally to this work

Correspondence: Wentao Kong; Wenping Wang, Email breezewen@163.com; puguang61@126.com

Video abstract

Point your SmartPhone at the code above. If you have a QR code reader the video abstract will appear. Or use: https://youtu.be/Q7-dXFhp0hI

Purpose: To develop and validate a reliable preoperative non-invasive diagnostic model for dual-phenotype hepatocellular carcinoma (DPHCC) by integrating multimodal imaging and clinical indicators, thereby facilitating clinical decision-making.

Patients and Methods: 222 pathologically confirmed patients (61 with DPHCC, 161 with non-DPHCC) were retrospectively enrolled in this study and randomly assigned to training and validation cohorts in an 8:2 ratio. Serological and multimodal imaging characteristics were analyzed. Univariate and multivariate logistic regression analyses identified independent DPHCC predictors and built a nomogram. Model performance and clinical utility were assessed by receiver operating characteristic (ROC) and decision curve analysis (DCA) curve respectively. The calibration curve was used to verify the model. Recurrence-free survival (RFS) was assessed using Kaplan-Meier and Log rank tests.

Results: In multivariate analysis, age (OR=0.91; P < 0.001), LDH (OR=1.03; P=0.002), PT (OR=0.14; P < 0.001), AFP (OR=4.04; P=0.019), Adler grade (OR=0.17; P=0.037), non-enhancing area (OR=8.30; P=0.004), arterial phase hyperenhancement (OR=0.12; P=0.015) and enhancing capsule (OR=0.32; P=0.04) were independent predictors of DPHCC. The nomogram achieved a robust predictive performance with C-index (0.92 vs 0.87) and accuracy (0.87 vs 0.86) in the training and validation cohorts. In addition, the calibration curve and DCA also showed good model performance. DPHCC patients had significantly lower RFS than non-DPHCC patients (P = 0.037).

Conclusion: A nomogram was established for non-invasive prediction of DPHCC risk utilizing multimodal imaging combined with clinical indicators to help achieve personalized treatment.

Keywords: dual-phenotype hepatocellular carcinoma, hepatocellular carcinoma, contrast enhanced magnetic resonance imaging, contrast enhanced ultrasound, combined model, nomogram

Introduction

The GLOBOCAN 2020 database revealed that primary liver cancer was the sixth most frequently diagnosed malignant tumor in the world, carrying the third highest mortality rate among all cancers. It accounted for 905,677 new cases and 830,180 deaths, posing a serious threat to human life and health.[1,2] There are three different pathological types of primary liver cancer, including hepatocellular carcinoma (HCC), intrahepatic cholangiocarcinoma (iCCA), and combined hepatocellular-cholangiocarcinoma (cHCC-CCA). HCC is the most common type, accounting for approximately 75–85% of cases.[1] In recent years, the treatment of HCC has experienced rapid advancements, leading to the establishment of an individualized comprehensive treatment model based on surgical interventions.[3] However, the long-term prognosis of

Received: 21 April 2025
Accepted: 20 June 2025
Published: 30 June 2025

patients remains unsatisfactory, with recurrence rates as high as 60–70% within 5 years after surgery.[4] There remains significant individual variation, indicating that HCC may have different biological subtypes. Dual-phenotype hepatocellular carcinoma (DPHCC), a subtype of HCC first reported in 2011, is clinically rare, accounting for about 10% of HCCs.[5] The histopathological morphology of DPHCC does not differ from that of typical HCC, but it is characterized by the simultaneous expression of any HCC marker (eg HepPar-1, pCEA, GPC-3, etc.. and any iCCA marker (eg CK19, CK7, MUC-1, etc.) within the same tumor cells as demonstrated on immunohistochemistry.[6] Due to its dual phenotype, DPHCC has a poorer prognosis and exhibits more frequent malignant biological behaviors, such as microvascular invasion (MVI) as well as intra- and extra-hepatic metastases, compared to non-DPHCC (NDPHCC).[7] Therefore, an accurate diagnosis of DPHCC can facilitate the optimization of clinical treatment choices. However, the routine imaging characteristics and clinical manifestations of DPHCC and NDPHCC are comparable, rendering preoperative imaging differential diagnosis highly challenging. Currently, the diagnosis of DPHCC primarily relies on postoperative immunohistochemical results, highlighting the urgent need for specific and non-invasive diagnostic methods to bridge this gap. Both ultrasonography (US) and magnetic resonance imaging (MRI) are recommended imaging screening methods for HCC, each of which has its own characteristics.[8] Without the use of contrast agent, US has the advantage of showing blood perfusion in the tumor by color Doppler. However, to our knowledge, there are no reports on the application of US in the diagnosis of DPHCC. Therefore, the objective of this study was to investigate the diagnostic value of preoperative multimodal imaging findings and clinical laboratory features for DPHCC.

Additionally, we sought to develop and validate a preoperative prediction model for DPHCC, which would facilitate non-invasive diagnosis as well as precise individualized medical treatment, thus enhancing the overall survival rate of patients with liver cancer.

Materials and Methods

Patients

This retrospective study was performed on patients diagnosed with DPHCC by surgical pathology at Zhongshan Hospital, Fudan University from January 2018 to January 2023. The inclusion criteria for DPHCC were as follows: (1) patients with DPHCC confirmed by postoperative pathological and immunohistochemical examination; (2) available contrast-enhanced magnetic resonance imaging (CEMRI) and contrast-enhanced ultrasound (CEUS) within two weeks before surgery; (3) complete clinical data. The exclusion criteria were as follows: (1) other antitumor treatments performed before image acquisition; (2) poor quality of CEUS or CEMRI data. A total of 61 DPHCC cases were included. We then randomly selected 244 patients with NDPHCC who were also pathologically diagnosed on the same day at a ratio of 1:4, and finally included 161 patients with NDPHCC according to the above exclusion criteria. Patients included in our study were randomly allocated to the training and validation cohorts in a ratio of 8:2 using the method of random number table Ethical approval for this retrospective study was obtained (B2022-223R), and informed consent was waived.

Clinical and Laboratory Data

Clinical and laboratory data were retrieved and recorded from the hospital record system. These included age, sex, cirrhosis, α-l-fucosidase (AFU), albumin (ALB), alanine aminotransferase (ALT), aspartate aminotransferase (AST), alkaline phosphatase (ALP), gamma-glutamyl transpeptidase (GGT), lactate dehydrogenase (LDH), prothrombin time (PT), platelets (PLT), carcinoembryonic antigen (CEA), α-fetoprotein (AFP), CA199 and hepatitis B surface antigen (HBsAg).

Pathological and Immunohistochemical Analyses

After fixation with formalin, the surgically resected specimens underwent pathologic examination and immunohistochemical analysis at the pathology department of Zhongshan Hospital, Fudan University. The diagnosis was made in accordance with the Standardized Pathological Diagnosis Guide for Primary Liver Cancer (2015).[6] The diagnostic criteria for DPHCC were consistent with those initially proposed in the literature:[5] (1) morphologically, typical HCC characteristics as defined by WHO were observed; (2) immunohistochemistry showed that more than 15% of tumor cells

concurrently expressed both hepatocytic and cholangiocytic markers. Please note the distinction of cHCC-CCA: Morphologically, it exhibits hybrid features of both HCC and iCCA, while immunohistochemically, the two tumor components express their respective specific markers—The HCC component expresses hepatocytic markers such as Hep Par-1, GPC-3, CD10, and Arg-1, whereas the iCCA component expresses cholangiocytic markers including CK7, CK19, and MUC-1. Pathological features were recorded including Edmondson-Steiner (ES) grade, the presence or absence of satellite and macroscopic cancer embolus, MVI and CK19 status. And we divided masses with ES grades I, I–II and II into the low-grade group and masses with grades II–III, III, III–IV and IV into the high-grade group.

Ultrasonography and Image Analyses

The grayscale ultrasound and CEUS examinations were performed by three ultrasound systems: Philips EPIQ7 unit (Philips, Bothell, WA, USA), LOGIQ E10 (GE Healthcare, Milwaukee, WI, USA) and Resona R9 Super (Mindray, Shenzhen, GD, China). The liver CEUS examinations performed in our center conformed to the standardized techniques recommended by the CEUS LI-RADS Technical Recommendations.[9] 1.2 mL SonoVue (Bracco Imaging, Milan, Italy) was injected into the antecubital vein, followed by 5 mL saline flush. Imaging was recorded on cine clips continuously for at least 60 seconds immediately after contrast administration and then scanned intermittently at 10–20 second intervals until the microbubbles were cleared from the circulation for up to 5 minutes. The imaging data were divided into arterial phase (AP, 10–45 s), portal venous phase (PVP, 45–120 s) and delayed phase (DP, >120 s). Only the largest lesion was chosen for the study, when there were multiple tumors in the liver. Two-dimensional ultrasound images provided data on tumor location, number, diameter, echogenicity (hypoechoic, isoechoic, hyperechoic, mixed), uniformity of echo distribution, boundary, shape, and blood flow classification.[10] CEUS images captured enhancement time parameters (start time, peaking time and iso-/hypo-enhancement times), enhancement patterns during AP, PVP and DP as well as non-enhancing area within tumors. The definitions of CEUS features were showed in Appendix 1. To ensure study quality, two sonographers with over 5 years of experience in liver ultrasonography independently reviewed the images, and any inconsistencies in their conclusions were resolved by a third sonographer with 10 years of experience, who made the final decision.

MRI and Images Analyses

All patients were scanned on a 1.5-T clinical MR scanner (Magnetom Area; Siemens Healthcare, Erlangen, Germany). Routine MRI sequences included non-enhanced T1-weighted (T1WI), T2-weighted (T2WI), and diffusion-weighted (DWI) imaging. The contrast agent dimeglumine gadopentetate (Gd-DTPA; Bayer HealthCare, Berlin, Germany) was administered at a total dose of 0.1 mmol/kg, followed by immediate flushing of 20 mL normal saline via a power syringe at a rate of 2 mL/s. AP, PVP, and DP were acquired at 20–30, 70–90, and 160–180 seconds after the injection of the contrast agent. The specific scanning settings were detailed in the Table S1. According to the Liver Imaging Report and Data System (LIRADS) version from 2018,[8] the main evaluations in MRI plain scan included: (1) signal uniformity of tumor (classified as homogeneous or heterogeneous); (2) presence or absence of lipid component. CEMRI involved evaluations on: (1) enhancement patterns during AP, PVP and DP; (2) APHE (non-rim arterial phase hyperenhancement of a lesion that is greater than the enhancement of the surrounding liver); (3) nonperipheral washout (partial or complete hypoenhancement within the lesion in the PVP or DP); (4) enhancing capsule (a hyper-enhanced structure surrounding the tumor during the PVP or DP); (5) heterogeneous enhancement.

Follow-Up

The follow-up protocol involved scheduled blood tests and contrast-enhanced image examinations initially at 1 month after surgery, then every 3 months during the first 2 years, shifting to every 6 months subsequently. When indeterminate results emerged, supplemental examinations such as bone scintigraphy or biopsies were performed to verify tumor recurrence. Recurrence was defined as radiologically or histologically confirmed intrahepatic HCC, tumor-in-vein, or distant metastasis. Recurrence-free survival (RFS) was calculated from the date of surgery to initial tumor recurrence or all-cause death. The data cutoff for our analysis was June 1, 2025.

Statistical Analyses

Statistical analyses were performed by R (version 4.3.2, http://www.r-project.org/) and IBM SPSS Statistics for Windows (version 20.0, IBM Corp), and. P< 0.05 was considered statistically significant. The quantitative data underwent a normality test. If the data satisfied the assumption of normality, it was presented as mean ± standard deviation (SD), and *t*-test was employed for comparing the two groups. In case the data did not meet the normality assumption, it was represented by median and interquartile range (IQR), and the Mann–Whitney *U*-test was used to compare between groups. Categorical variables were expressed as counts and percentages, with group comparisons performed using Chi-square test or Fisher's exact test. Univariate and multivariate logistic regression was performed using stepwise backward LR methods, excluding a P-value criterion of > 0.1, to identify independent predictors of DPHCC. To visualize the results, we utilized the 'rms' package in R software to construct a nomogram model. Internal consistency was assessed through bootstrap validation (1000 repetitions) and demonstrated by calibration curves. The predictive performance of the nomogram model was evaluated using receiver operating characteristic (ROC) curves. Its clinical utility was quantified through decision curve analysis (DCA), and the predictive accuracy was tested using calibration curve. RFS was estimated via Kaplan-Meier curves, and intergroup differences were assessed with the Log rank test.

Results

Demographics and Clinical Characteristics

Finally, 222 patients who met the inclusion criteria were included (Figure 1), including 193 males and 29 females, aged from 27 to 93 (56 ± 12) years. 61 cases were DPHCC (50 males and 11 females), and 161 patients were NDPHCC (143 males and 18 females). Compared to the NDPHCC group, the DPHCC group exhibited a younger age (50 ± 12 years vs 58 ± 12 years). Serologically, the level of AFU, ALP, LDH and AFP as well as the positive rate of HBsAg were higher while the PT level was lower in DPHCC group. All of the above differences were significant (P < 0.05) (Table S2). Pathologically, in the DPHCC vs NDPHCC group, the incidence of high-ES grade, satellite lesion and cancer embolism were 72.1% vs 13.7% (P = 0.000), 11.5% vs 3.1% (P = 0.033) and 18.0% vs 0.0% (P= 0.000). In addition, the results showed that the positive rate of CK19 and MVI in the DPHCC vs NDPHCC group were 98.4% vs 19.9% (P = 0.000) and 55.7% vs 24.2% (P = 0.000), respectively (Figure S1). Subsequently, 222 patients were randomly divided into a training cohort (45 DPHCC, 133 NDPHCC) and a validation cohort (16 DPHCC, 28 NDPHCC). Among the DPHCC patients in the training cohort, there were 36 males and 9 females, ranging age from 27 to 76 (50 ± 12) years old. Among the NDPHCC patients in the training cohort, there were 120 males and 13 females, aged from 28 to 93 (59 ± 12) years old. The baseline characteristics of patients in the training cohort and the validation cohort were shown in Table 1.

Ultrasonic and MRI Characteristics

In terms of ultrasonographic manifestations, the DPHCC group exhibited larger tumor diameters and a higher incidence of non-enhancing areas compared to the NDPHCC group (41 vs 30mm, 41.0% vs 10.6%, P < 0.05, respectively). Among the MRI features, heterogeneous enhancement and persistent enhanced type (hyper-hyper-hyper) were more common in the DPHCC group than those in the NDPHCC group (42.6% vs 24.1%, 24.6% vs 6.8%, all P= 0.001). While the incidence of lipid components, wash-in and wash-out enhanced type (hyper-low-low), APHE, nonperipheral washout and enhancing capsule were lower than those in the NDPHCC group (1.6% vs 12.4%, 73.8% vs 91.3%, 75.4% vs 96.3%, 73.8% vs 94.4%, 42.6% vs 71.4%, all P <0.05). The imaging characteristics of DPHCC and NDPHCC were described in Table S3 and Figures 2–3.

Univariate and Multivariable Logistic Regression Analyses and Nomogram Construction

Variables with P <0.1 were included in multivariable logistic regression as candidate predictors associated with DPHCC. Multivariate logistic regression analysis indicated that age (odds ratio [OR] = 0.91; P < 0.001), LDH (OR = 1.03; P = 0.002), PT (OR = 0.14; P < 0.001), AFP (OR = 4.04; P=0.019), Adler grade (OR = 0.17; P = 0.037), non-enhancing area (OR = 8.30; P = 0.004), APHE (OR = 0.12; P = 0.015) and enhancing capsule (OR = 0.32; P = 0.04) were independent

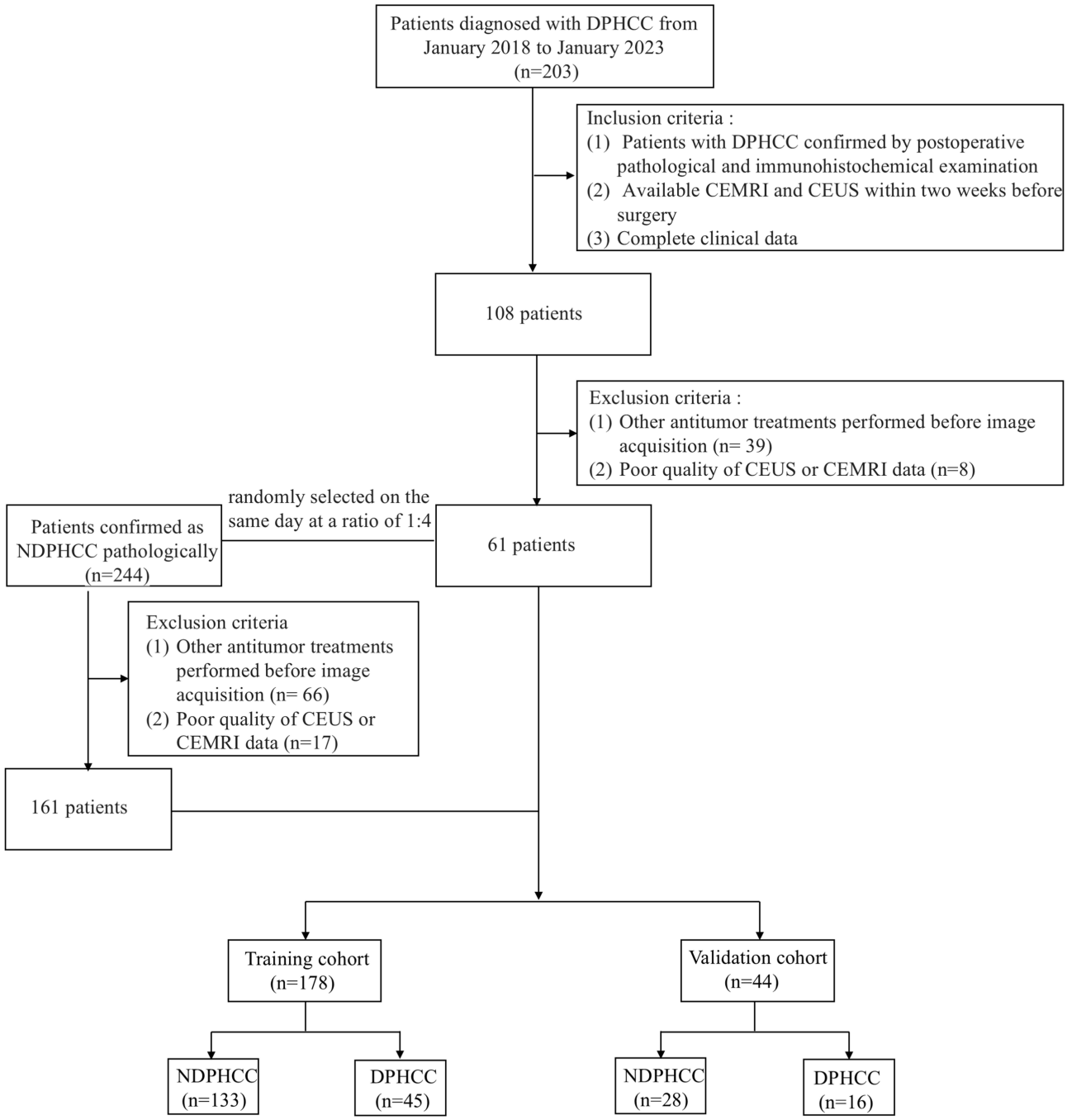

Figure 1 The flowchart of patient inclusion and exclusion.

influence factors of DPHCC, and these independent predictors were used to construct the DPHCC estimation nomogram (Figure 4). The results of univariate and multivariable logistic regression analyses of variables were shown in Table 2.

Evaluation and Validation of DPHCC Prediction Model

The results showed that the nomogram had a good ability to distinguish DPHCC from NDPHCC with a C-index (0.92 vs 0.87) and accuracy (0.87 vs 0.86) in the training and validation cohorts (Figure 5A and B). In addition, using 0.25 and 0.42 as the cutoff score, the sensitivity, specificity, PPV and NPV were 0.89, 0.86, 0.68 and 0.96 in the training cohort and 0.81, 0.89, 0.81 and 0.89 in the validation cohort, respectively (Table 3). The utility and clinical value of the

https://doi.org/10.2147/JHC.S533963

Table 1 Baseline Characteristics of Training and Validation Cohorts

Variables	Training Cohort (n = 178)	Validation Cohort (n = 44)	P value
Clinical features			
Age (y)	56.7 ± 12.3	53.9 ± 12.1	0.188
Sex			0.532
Male	156 (87.6)	37 (84.1)	
Female	22 (12.4)	7 (15.9)	
Cirrhosis			0.249
Yes	92 (51.7)	27 (61.4)	
No	86 (48.3)	17 (38.6)	
Fatty liver			0.611
Yes	42 (23.6)	12 (27.3)	
No	136 (76.4)	32 (72.7)	
AFU (U/L)	30.3 (27.0–35.5)	31.9 (28.5–37.5)	0.149
ALB (g/L)	44.0 (41.0–46.0)	43.0 (41.0–45.0)	0.678
ALT (U/L)	26.5 (18.0–42.0)	32.0 (21.0–43.8)	0.274
AST (U/L)	26.0 (20.0–36.0)	28.0 (22.3–37.8)	0.227
ALP (U/L)	71.0 (60.0–88.3)	81.5 (65.3–99.0)	0.115
GGT (U/L)	39.0 (22.8–75.0)	37.5 (23.3–67.8)	0.992
LDH (U/L)	178.0 (158.0–199.3)	190.5 (163.3–222.8)	0.072
PT (s)	12.0 (11.6–12.4)	11.9 (11.5–12.6)	0.834
PLT (*10^9/L)	163.5 (126.8–199.5)	154.0119.0–206.8)	0.528
CEA (ng/mL)	2.4 (1.6–3.8)	2.4 (1.5–3.3)	0.437
AFP (ng/mL)			0.965
<400	137 (77.0)	34 (77.3)	
≥400	41 (23.0)	10 (20.7)	
CA199 (U/mL)			0.753
<34	153 (86.0)	37 (84.1)	
≥34	25 (14.0)	7 (15.9)	
HBsAg			0.353
Positive	125 (70.2)	34 (77.3)	
Negative	53 (29.8)	10 (22.7)	
Pathological features			
Edmondson-Steiner grade			0.149
Low-grade	129 (72.5)	27 (61.4)	
High-grade	49 (27.5)	17 (38.6)	
CK19			0.345
Positive	71 (39.9)	21 (47.7)	
Negative	107 (60.1)	23 (52.3)	
MVI			0.206
Positive	55 (30.9)	18 (40.9)	
Negative	123 (69.1)	26 (59.1)	
Satellite			1.000
Yes	10 (5.6)	2 (4.5)	
No	168 (94.4)	42 (95.5)	
Cancer embolus			1.000
Yes	9 (5.1)	2 (4.5)	
No	169 (94.9)	42 (95.5)	

(*Continued*)

Table 1 (Continued).

Variables	Training Cohort (n = 178)	Validation Cohort (n = 44)	P value
Ultrasonic features of tumor			
Location			**0.025**
Right lobe	127 (71.3)	25 (56.8)	
Left lobe	39 (21.9)	18 (40.9)	
Across two lobes	10 (5.6)	0 (0.0)	
Caudate lobe	2 (1.1)	1 (2.3)	
Number			0.809
Single	157 (88.2)	40 (90.9)	
Multiple	21 (11.8)	4 (9.1)	
Diameter (mm)	30.0 (20.0–45.0)	30.0 (20.0–51.0)	0.958
Echogenicity			**0.024**
Hypoechoic	121 (68.0)	31 (70.5)	
Isoechoic	10 (5.6)	8 (18.2)	
Hyperechoic	35 (19.7)	4 (9.1)	
Mixed	12 (6.7)	1 (2.3)	
Echo uniformity			0.867
Homogeneous	119 (66.9)	30 (68.2)	
Heterogeneous	59 33.1)	14 (31.8)	
Boundary			0.253
Clear	94 (52.8)	19 (43.2)	
Unclear	84 (47.2)	25 (56.8)	
Shape			0.833
Regular	98 (55.1)	25 (56.8)	
Irregular	80 (44.9)	19 (43.2)	
Adler grade			0.160
0	52 (29.2)	18 (40.9)	
I	30 (16.9)	6 (13.6)	
II	72 (40.4)	11 (25.0)	
III	24 (13.5)	9 (20.5)	
Enhancement time (s)			
Start time	16.0 (14.0–20.0)	17.0 (13.3–20.0)	0.551
Peaking time	23.0 (20.0–27.0)	24.0 (21.3–28.8)	0.158
Iso-enhancement time	34.0 (30.0–40.3)	35.5 (30.0–40.0)	0.540
Hypo-enhancement time	60.0 (42.0–100.0)	64.0 (44.3–113.8)	0.697
CEUS enhancement pattern			0.976
Hyper-low-low	111 (62.4)	28 (63.6)	
Hyper-iso-low	46 (25.8)	12 (27.3)	
Hyper-iso-iso	20 (11.2)	4 (9.1)	
Hyper-hyper-hyper	1 (0.6)	0 (0.0)	
Non-enhanced area			0.250
Yes	31 (17.4)	11 (25.0)	
No	147 (82.6)	33 (75.0)	
MRI features of tumor			
Signal uniformity			0.167
Homogeneous	139 (78.1)	30 (68.2)	
Heterogeneous	39 (21.9)	14 (31.8)	
Lipid components			0.126
Yes	20 (11.2)	1 (2.3)	
No	158 (88.8)	43 (97.7)	

(*Continued*)

Table 1 (Continued).

Variables	Training Cohort (n = 178)	Validation Cohort (n = 44)	P value
CEMRI enhancement pattern			0.503
Hyper-low-low	155 (87.1)	37 (84.1)	
Hyper-iso-iso	2 (1.1)	0 (0.0)	
Hyper-hyper-low	1 (0.6)	1 (2.3)	
Hyper-hyper-hyper	20 (11.2)	6 (13.6)	
APHE			0.703
Yes	160 (89.9)	41 (93.2)	
No	18 (10.1)	3 (6.8)	
Nonperipheral washout			0.772
Yes	159 (89.3)	38 (86.4)	
No	19(10.7)	6(13.6)	
Enhancing capsule			0.496
Yes	115 (64.6)	26 (59.1)	
No	63 (35.4)	18 (40.9)	
Heterogeneous enhancement			0.140
Yes	52 (29.2)	8 (18.2)	
No	126 (70.8)	36 (81.8)	

Notes: Data are numbers (%), means ± SD, or medians (ranges). Bold values are variables with $p < 0.05$.

nomogram was evaluated through decision curve analysis (Figure 5C and D). The results demonstrated that the nomogram achieved a higher net benefit over a wider range of threshold probability (2% to 100% in the training cohort and 9% to 100% in the validation cohort). The approximate distribution of the calibration curve along the reference line indicated a good agreement between the estimation of DPHCCC aspects and pathological results using this model (Figure 6). The P-values of Hosmer-lemeshow test in the training cohort (0.210) and validation cohort (0.682) were both greater than 0.05, indicating that the predicted probability of the model fitted the actual probability well. These reflected good discriminability, calibration and clinical practicability of the model.

In clinical application, 0.25 and 0.42 were used as cut-off values, and sensitivity, specificity, positive predictive value, negative predictive and accuracy value were summarized to evaluate the quality of the model. In our study, 86% of patients in the training group and 89% in the validation group were able to correctly diagnose DPHCC.

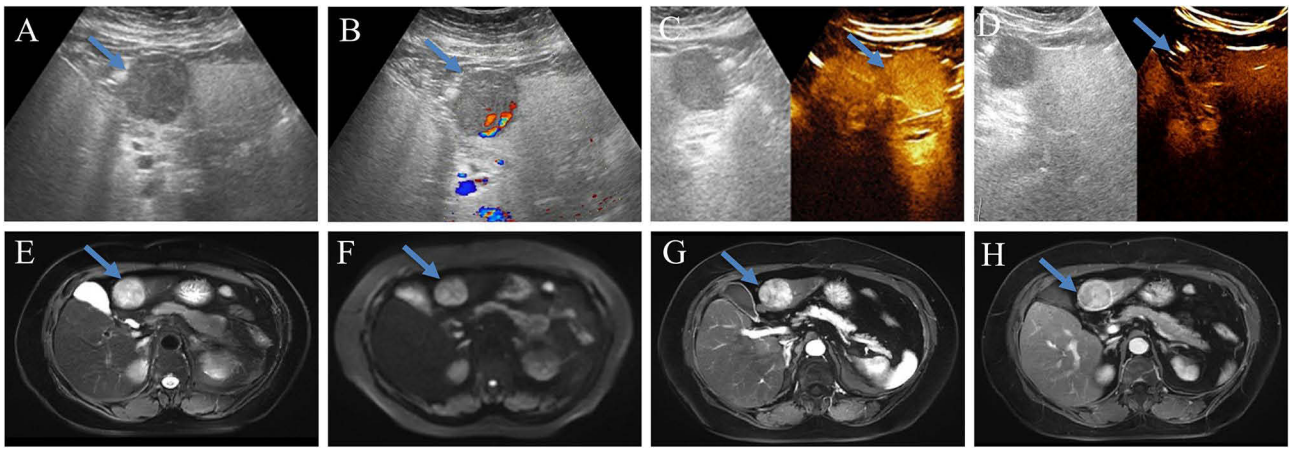

Figure 2 A 77-year-old woman with NDPHCC in the left outer lobe, and the mass was indicated by the blue arrow. (**A**) Grayscale ultrasound showed a hypoechoic, homogeneous and regular tumor. (**B**) Color Doppler imaging showed a grade III blood flow. (**C**) The arterial phase of CEUS showed uniform and significant enhancement. (**D**) The delayed phase showed low enhancement. (**E**) T2-weighted image showed a mass with higher signal. (**F**) Diffusion-weighted image (b = 500) showed a high signal mass. (**G**) The CEMRI showed significantly enhancement in arterial phase. (**H**) The delayed phase showed low enhancement and enhancing capsule.

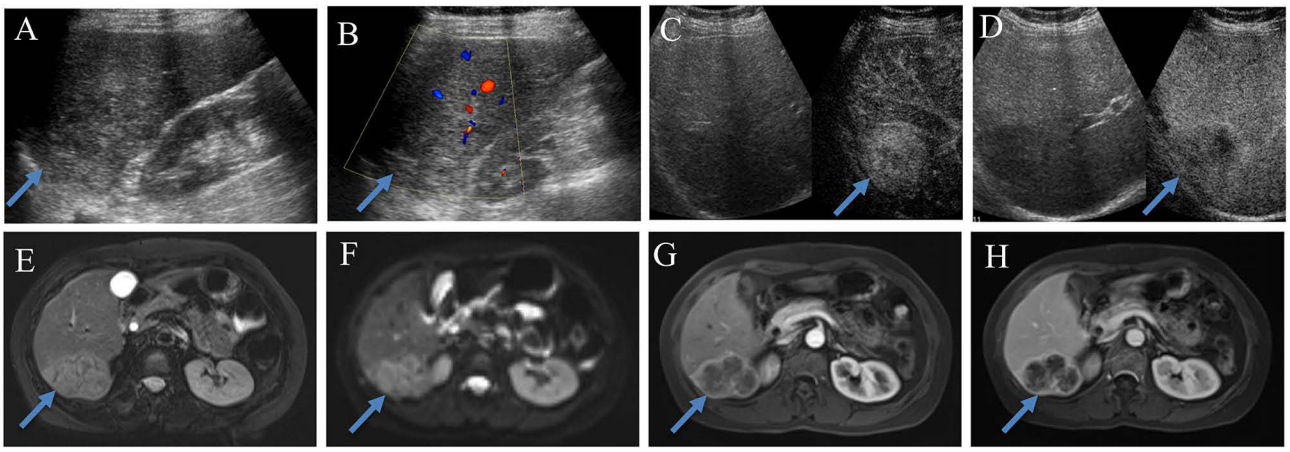

Figure 3 A 51-year-old woman with DPHCC in the right posterior lobe, and the mass was indicated by the blue arrow. (**A**) Grayscale ultrasound showed a hypoechoic, heterogeneous and irregular tumor. (**B**) Color Doppler imaging showed a grade I blood flow. (**C**) The arterial phase of CEUS showed uneven hyper-enhancement and non-enhancing area. (**D**) The delayed phase showed low enhancement and non-enhancing area. (**E**) T2-weighted image showed a moderately high signal mass with slightly higher signal margins. (**F**) Diffusion-weighted image (b = 500) showed a high signal ring in the periphery of the mass and a slightly higher signal in the center. (**G**) The arterial phase showed rim-APHE. (**H**) The portal venous phase showed mild decreased enhancement.

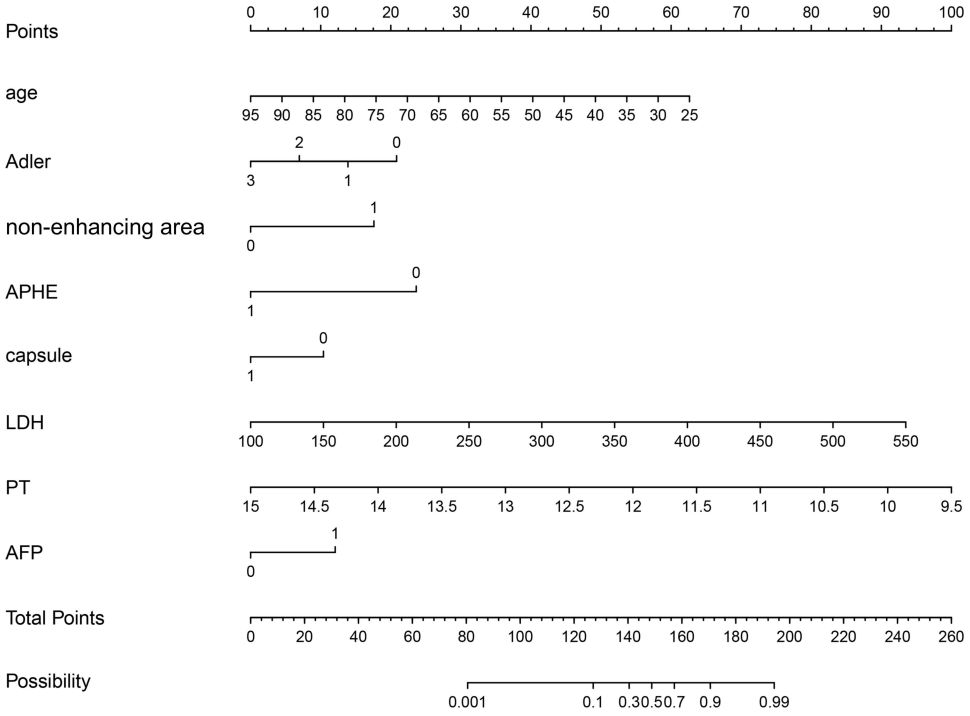

Figure 4 Nomogram for DPHCC prediction. The column chart for predicting DPHCC was created based on the 8 predictors above. To use a nomogram, place each patient's value on each variable axis and draw a line up to determine the number of points received for each variable value. The sum of these numbers is located on the total point axis and a line is drawn down on the bottom axis to determine the probability of DPHCC.

RFS Analysis

A total of 155 patients with follow-up data were included in the RFS analysis, comprising 44 DPHCC cases and 111 NDPHCC cases. The DPHCC group demonstrated a median follow-up duration of 69.1 months (IQR: 62.9–75.3) with 22 recurrence cases (50.0%), while the NDPHCC group showed a median follow-up of 62.7 months (IQR: 58.1–67.2) with 41 recurrence cases (36.9%). The 1-, 2-, and 5-year RFS rates were 72.5%, 53.4%, and 42.9% for DPHCC patients, compared to 86.5%, 74.4%, and 57.8% for NDPHCC patients, respectively (Figure S2). Log rank test analysis revealed statistically significant difference in RFS between the two groups (P = 0.037).

https://doi.org/10.2147/JHC.S533963

Table 2 Value of Univariate and Multivariate Analysis in the Diagnosis of DPHCC

Variables	Univariate Analysis		Multivariate Analysis	
	OR (95% CI)	P value	OR (95% CI)	P value
Age	0.94 (0.91–0.97)	<0.001	0.91 (0.86–0.96)	<0.001
AFU	1.07 (1.02–1.11)	0.004		
ALP	1.01 (1.00–1.02)	0.024		
LDH	1.01 (1.01–1.02)	<0.001	1.03 (1.01–1.04)	0.002
PT	0.39 (0.23–0.68)	<0.001	0.14 (0.05–0.36)	<0.001
AFP	4.94 (2.34–10.63)	<0.001	4.04 (1.26–12.9)	0.019
HBsAg	2.37 (1.06–5.85)	0.046		
Diameter (mm)	1.02 (1.00–1.03)	0.010		
Adler grade		0.164		0.037
0	Reference		Reference	
II	0.46 (0.21–1.02)	0.055	0.21 (0.06–0.76)	0.017
III	0.35 (0.10–1.17)	0.088	0.17 (0.03–0.90)	0.037
Enhancement time (s)				
Iso-enhancement time	0.97 (0.94–1.00)	0.057		
Non-enhanced area	6.15 (2.72–14.35)	<0.001	8.30 (2.00–34.41)	0.004
CEMRI enhancement pattern				
Hyper-low-low	Reference			
Hyper-hyper-hyper	3.56 (1.37–9.25)	0.009		
APHE	0.10 (0.03–0.27)	<0.001	0.12 (0.02–0.66)	0.015
Nonperipheral washout	0.20 (0.07–0.53)	0.001		
Enhancing capsule	0.28 (0.14–0.56)	<0.001	0.32 (0.11–0.95)	0.040
Heterogeneous enhancement	2.88 (1.41–5.88)	0.004		

Discussion

DPHCC is a rare subtype of HCC that shows higher aggressiveness, proliferation and migration ability.[11–13] In the existing literature reports, there is still a scarcity of the preoperative imaging features of DPHCC, with the majority of the focus being on the features of CEMRI.[13–16] Recently, there have also been reports of preoperative prediction of DPHCC using the CEMRI radiomics analysis.[17,18] To the best of our knowledge, this is the first predictive model that utilizes a combination of multimodal imaging and clinical serological features.

In this study, the nomogram achieved a robust predictive performance in the training and validation cohorts. In addition, calibration and DCA curves also showed good performance of the nomogram. In clinical application, 86% and 89% of patients in the training group and validation group were able to correctly diagnose DPHCC, respectively, providing a new method for non-invasive prediction of DPHCC before surgery, which can help doctors choose more appropriate treatment methods before surgery.

US is the most widely used modality for HCC screening and surveillance.[19] We found that two ultrasound features, low Alder grade and the presence of non-enhancing areas of the tumor, were independent predictors of DPHCC. Compared to Adler grade 0, the OR of grade II and grade III was 0.21 and 0.17, respectively, indicating that the more abundant blood flow in the tumor, the stronger the diagnosis of NDPHCC. And the OR value of non-enhancing area was as high as 8.3. These features further reflect that DPHCC is a tumor with poor blood supply, and the reduction of blood vessels further aggravates the hypoxic microenvironment of the tumor, making it more likely to metastasize. Postoperative pathology showed higher positive rates of CK19 and MVI as well as increased incidences of satellite nodules and intravascular cancer thrombus in the DPHCC group. Moreover, our study revealed that the RFS rates of DPHCC was lower compared to NDPHCC ($P < 0.05$), further confirming the highly aggressive nature and elevated recurrence probability of this HCC subtype. Li et al indicated that elevated tumor-associated lymphatic vessel density levels predict poorer prognosis in hepato-biliary-pancreatic patients following radical resection.[20] Studies[21] have shown that HCC development is related to the increase of tumor vessels and arterialization due to the pro-angiogenic factors by

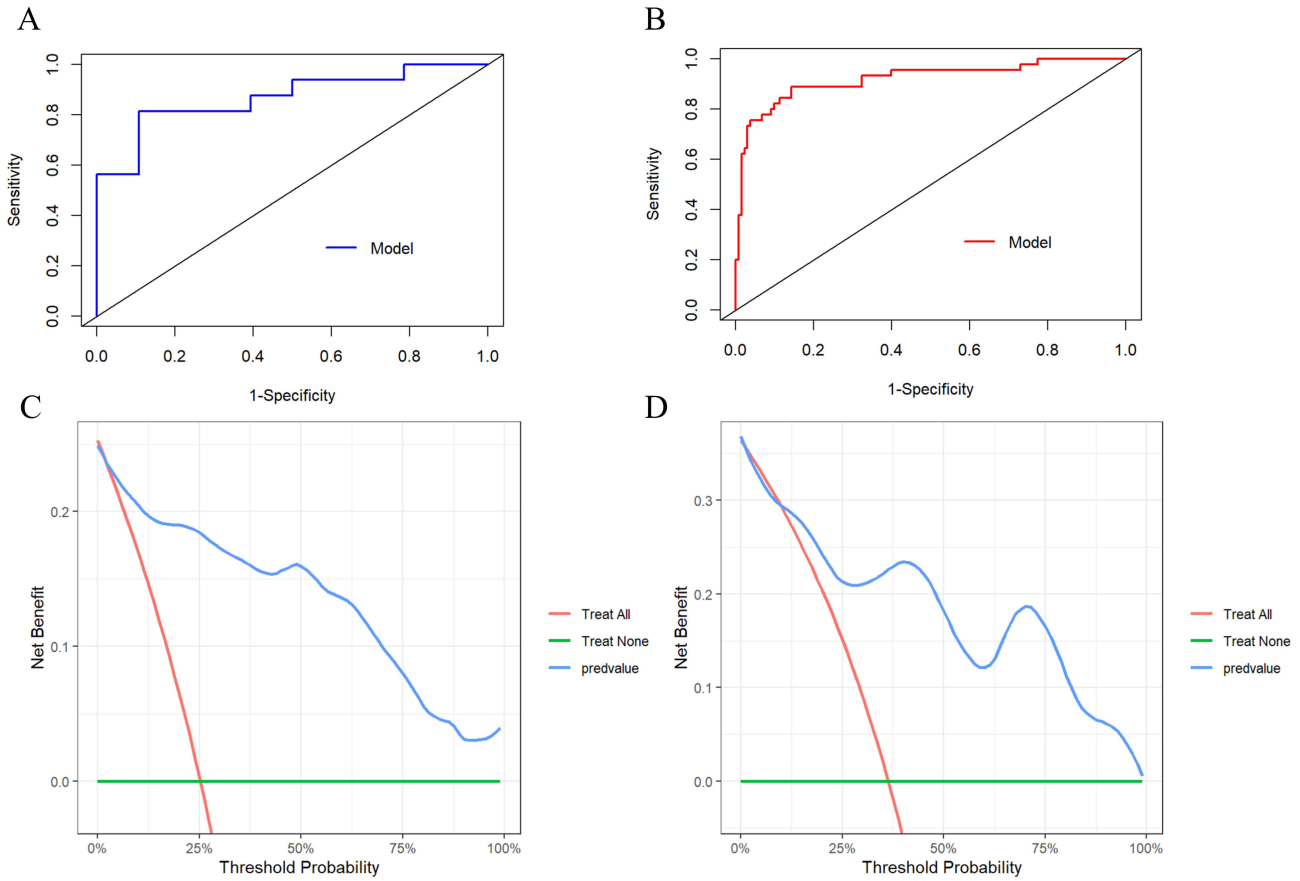

Figure 5 Receiver operating characteristic (ROC) curve and decision curve analysis (DCA) of the training and validation cohorts. (**A**) ROC curve of the training cohort. (**B**) ROC curve of the validation cohort. (**C**) DCA of the training cohort. (**D**) DCA of the validation cohort. The nomogram had good discriminative performance, and the area under ROC curve (AUC) in the training and validation cohorts were 0.92 and 0.87, respectively. The DCA showed that when the threshold probabilities for patients in our study were 2–100% and 9%-100%, respectively, using a nomogram to predict DPHCC was more beneficial than treating all patients or treating none.

various molecular pathways (such as HIF, STAT and NF-κB, etc), while the intensification of hypoxia in DPHCC forms a vicious cycle, thus ultimately forming its high malignancy.

Our multivariate logistic regression results showed that the presence of non-APHE (rim-APHE) in the AP and the absence of enhancing capsule in the PVP or DP were independent predictive factors for DPHCC, with OR values (95% CI) of 0.12 (0.02 ~ 0.66) and 0.32 (0.11 ~ 0.95), respectively. APHE and enhancing capsule is one of the main imaging features for the diagnosis of HCC in LI-RADS, and the mechanism may be attributed to the growth of tumor cells, angiogenesis and fibrous desmoplasia around tumor.[8] Previous studies[22,23] have shown that the presence of tumor capsule is a favorable prognostic factor for HCC. Some studies[24,25] have shown that rim-APHE is more common in iCCA as well

Table 3 Diagnostic Performance of Nomogram in Prediction of DPHCC

Variables	Training Cohort	Validation Cohort
AUC/C-Index	0.92	0.87
Cutoff score	0.25	0.42
Sensitivity (95% CI)	0.89 (0.76–0.96)	0.81 (0.54–0.96)
Specificity (95% CI)	0.86 (0.79–0.91)	0.89 (0.72–0.98)
PPV (95% CI)	0.68 (0.54–0.79)	0.81 (0.54–0.96)
NPV (95% CI)	0.96 (0.90–0.99)	0.89 (0.72–0.98)
Accuracy (95% CI)	0.87 (0.81–0.91)	0.86 (0.73–0.95)

https://doi.org/10.2147/JHC.S533963

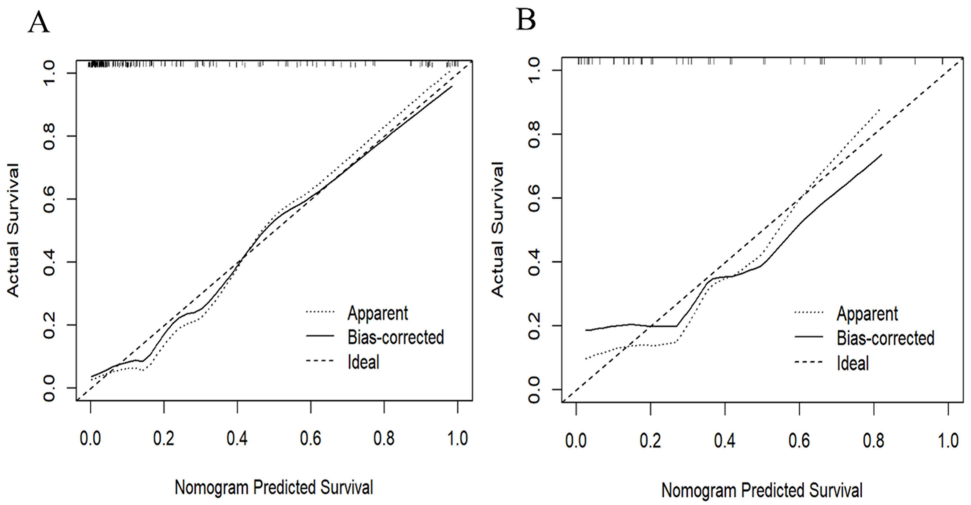

Figure 6 Calibration curves comparing predicted and actual DPHCC probabilities. (**A**) Calibration curve of the nomogram in the training cohort. (**B**) Verify the calibration curve of the nomogram in the validation cohorts. The calibration curve describes the agreement between the predicted DPHCC probability and the observed DPHCC results. The X-axis represents the predicted probability of DPHCC. The Y-axis represents the actual DPHCC probability. The long-dotted line represents the perfect prediction of the ideal model. The short-dashed line indicates the predicted value of the column graph, and the solid line indicates the estimated value after bootstrap correction. A well-calibrated curve for a nomogram will be close to the ideal line.

as cHCC-CCA, and is less common in HCC. HCC with rim-APHE has a more prominent hypoxic and fibrotic tumor microenvironment, faster tumor growth, and more frequent early recurrence. These predictive factors suggest that DPHCC is an aggressive tumor with MRI imaging features similar to iCCA, which is consistent with previous finding.[15] The incidence of hyper-hyper-hyper enhancement in CEMRI was higher in the DPHCC group than that in the NDPHCC group. This suggested that the enhancement pattern observed in most DPHCCS was sustained, resembling the imaging characteristics of iCCA, rather than the typical wash-in and wash-out pattern of HCC. However, we excluded them after multivariate regression analysis, suggesting that their role in predicting the occurrence of DPHCC was limited. Therefore, further studies with larger sample sizes were still needed to confirm these findings.

In terms of clinical characteristics, we found that the younger the patient, the higher the probability of developing DPHCC, which may be related to the co-expression of CK19 and GPC3. Studies[13,26] have shown that CK19 and GPC3 are highly expressed in younger HCC patients, and their co-expression is associated with more aggressive disease and poorer prognosis. In terms of clinical serological characteristics, we found that DPHCC patients have a high level of LDH. Yan et al[27] have shown that LDH, a glycolytic enzyme present in various tissues and tumors in the human body, can provide anaerobic conditions for tumor cells, thereby promoting cancer progression. Therefore, our findings further support the notion that DPHCC is a hypoxic tumor. Serum AFP has become the most widely used marker in the diagnosis of HCC, and its elevation is usually associated with poor cell differentiation and tumor metastasis. Hong Wei et al[28] found that AFP level > 400 ng/mL is one of the factors that can predict early postoperative recurrence. Our study found that AFP ≥ 400 ng/mL was an independent predictive factor for DPHCC, while CEA and CA199 were not significant in both univariate and multivariate regression analyses. In addition, the shortening of PT is also an independent predictive factor for DPHCC. Some literatures[29] have shown that the shortening of PT is a predictor of portal vein thrombosis, which also suggested that DPHCC is highly malignant and prone to metastasis. Based on these findings, we conclude that clinically and serologically DPHCC is more inclined to the presentation of HCC, but has a worse prognosis compared to HCC.

This study also had some limitations: Firstly, it was a retrospective study, and there might lead to selection bias. Secondly, this study was a single-center study, the sample size of DPHCC was limited, and no external validation was conducted, so future multi-center and large-sample studies were needed to further validate the accuracy of the formula method. In addition, due to the lack of endpoint data on overall survival, we were unable to conduct the analysis of overall survival. And further investigation into imaging, clinical and prognostic differences of various immunohistochemical markers, including CK7 and CK19, is warranted in the future.

Conclusion

In conclusion, we established a reliable model for preoperative prediction of DPHCC by utilizing eight indicators with excellent predictive performance. It offers a non-invasive and convenient approach for preoperative clinical decision-making as well as individualized treatment, thereby providing clinicians with valuable insights.

Abbreviations

AP, Arterial phase; APHE, Arterial phase hyperenhancement; AUC, Area under the ROC curve; CEMRI, Contrast-enhanced magnetic resonance imaging; CEUS, Contrast-enhanced ultrasound; DCA, Decision curve analysis; DP, Delayed phase; DPHCC, Dual-phenotype hepatocellular carcinoma; ES, Edmondson-Steiner; iCCA, Intrahepatic cholangiocarcinoma; MVI, Microvascular invasion; NDPHCC, Non-dual-phenotype hepatocellular carcinoma; OR, Odds ratio; PVP, Portal venous phase; RFS, Recurrence-free survival; ROC, Receiver operating characteristic.

Data Sharing Statement

The raw data supporting the conclusions of this article will be made available by the authors, without undue reservation.

Ethics Statement

The studies were reviewed and approved by the Institutional Review Board of Zhongshan Hospital Affiliated to Fudan University (B2022-223R). The study adhered to the principles of the Declaration of Helsinki. Given the retrospective observational nature of the study without involving any direct patient contact or intervention, the informed consent was waived with the permission of the ethics committee. Patient records/information was anonymized and de-identified prior to analysis.

Acknowledgments

We thank Jianyi Qu for his help in the feature analysis of magnetic resonance images.

Author Contributions

All authors made a significant contribution to the work reported, whether that is in the conception, study design, execution, acquisition of data, analysis and interpretation, or in all these areas; took part in drafting, revising or critically reviewing the article; gave final approval of the version to be published; have agreed on the journal to which the article has been submitted; and agree to be accountable for all aspects of the work.

Funding

This work was supported by National Natural Science Foundation of China (Grant No. 82272013 and No. 82472004), Clinical Research Plan of SHDC (Grant No. SHDC2020CR1031B) and Clinical Trials from the Affiliated Drum Tower Hospital, Medical School of Nanjing University (2022-LCYJ-MS-24). All funding departments had no role in the collection, analysis, or interpretation of the data or in the decision to submit the manuscript for publication.

Disclosure

The authors report no conflicts of interest in this work.

References

1. Sung H, Ferlay J, Siegel RL, et al. Global cancer statistics 2020: GLOBOCAN estimates of incidence and mortality worldwide for 36 cancers in 185 countries. *CA Cancer J Clin*. 2021;71(3):209–249. doi:10.3322/caac.21660
2. Yu Z, Bai X, Zhou R, et al. Differences in the incidence and mortality of digestive cancer between global cancer observatory 2020 and global burden of disease 2019. *Int J Cancer*. 2024;154(4):615–625. doi:10.1002/ijc.34740
3. Wang QB, Li J, Zhang ZJ, et al. The effectiveness and safety of therapies for hepatocellular carcinoma with tumor thrombus in the hepatic vein, inferior vena cave and/or right atrium: a systematic review and single-arm meta-analysis. *Expert Rev Anticancer Ther*. 2025;25(5):561–570. doi:10.1080/14737140.2025.2489651
4. Xu XF, Xing H, Han J, et al. Risk factors, patterns, and outcomes of late recurrence after liver resection for hepatocellular carcinoma: a multicenter study from China. *JAMA Surg*. 2019;154(3):209–217. doi:10.1001/jamasurg.2018.4334

5. Lu XY, Xi T, Lau WY, et al. Hepatocellular carcinoma expressing cholangiocyte phenotype is a novel subtype with highly aggressive behavior. *Ann Surg Oncol*. 2011;18(8):2210–2217. doi:10.1245/s10434-011-1585-7
6. Cong WM, Bu H, Chen J, et al. Practice guidelines for the pathological diagnosis of primary liver cancer: 2015 update. *World J Gastroenterol*. 2016;22(42):9279–9287. doi:10.3748/wjg.v22.i42.9279
7. Zhang J, Qi YP, Ma N, et al. Overexpression of epcam and CD133 correlates with poor prognosis in dual-phenotype hepatocellular carcinoma. *J Cancer*. 2020;11(11):3400–3406. doi:10.7150/jca.41090
8. Marrero JA, Kulik LM, Sirlin CB, et al. Diagnosis, staging, and management of hepatocellular carcinoma: 2018 practice guidance by the American association for the study of liver diseases. *Hepatology*. 2018;68(2):723–750. doi:10.1002/hep.29913
9. Elsayes KM, Kielar AZ, Chernyak V, et al. LI-RADS: a conceptual and historical review from its beginning to its recent integration into AASLD clinical practice guidance. *J Hepatocell Carcinoma*. 2019;6:49–69. doi:10.2147/JHC.S186239
10. Adler DD, Carson PL, Rubin JM, Quinn-Reid D. Doppler ultrasound color flow imaging in the study of breast cancer: preliminary findings. *Ultrasound Med Biol*. 1990;16(6):553–559. doi:10.1016/0301-5629(90)90020-D
11. Liu LZ, Yang LX, Zheng BH, et al. CK7/CK19 index: a potential prognostic factor for postoperative intrahepatic cholangiocarcinoma patients. *J Surg Oncol*. 2018;117(7):1531–1539. doi:10.1002/jso.25027
12. Ouyang X, Yan Y, Zhang S, Li M, Li M, Liu Q. Microvascular invasion is associated with poor survival in patients with dual-phenotype hepatocellular carcinoma. *Am J Clin Pathol*. 2024;161(3):245–255. doi:10.1093/ajcp/aqad143
13. Huang K, He Y, Liang T, et al. Analysis of clinicopathologic and imaging features of dual-phenotype hepatocellular carcinoma. *Sci Rep*. 2024;14(1):3314. doi:10.1038/s41598-024-53831-5
14. Wu Q, Yu YX, Fan YF, et al. The prediction value of enhanced magnetic resonance imaging nomogram model for dual phenotype hepatocellular carcinoma. *Zhonghua Yi Xue Za Zhi*. 2022;102(15):1086–1092. doi:10.3760/cma.j.cn112137-20211030-02406
15. Gu HX, Huang XS, Xu JX, Zhu P, Xu JF, Fan SF. Diagnostic value of MRI features in dual-phenotype hepatocellular carcinoma: a preliminary study. *J Digit Imaging*. 2023;36(6):2554–2566. doi:10.1007/s10278-023-00888-9
16. Liu MT, Zhang JY, Xu L, et al. A multivariate model based on gadoxetic acid-enhanced MRI using Li-RADS v2018 and other imaging features for preoperative prediction of dual-phenotype hepatocellular carcinoma. *Radiol Med*. 2023;128(11):1333–1346. doi:10.1007/s11547-023-01715-5
17. Huang X, Long L, Wei J, et al. Radiomics for diagnosis of dual-phenotype hepatocellular carcinoma using Gd-EOB-DTPA-enhanced MRI and patient prognosis. *J Cancer Res Clin Oncol*. 2019;145(12):2995–3003. doi:10.1007/s00432-019-03062-3
18. Wu Q, Yu YX, Zhang T, et al. Preoperative diagnosis of dual-phenotype hepatocellular carcinoma using enhanced MRI radiomics models. *J Magn Reson Imaging*. 2023;57(4):1185–1196. doi:10.1002/jmri.28391
19. Omata M, Cheng AL, Kokudo N, et al. Asia-Pacific clinical practice guidelines on the management of hepatocellular carcinoma: a 2017 update. *Hepatol Int*. 2017;11(4):317–370. doi:10.1007/s12072-017-9799-9
20. Li J, Liang YB, Wang QB, et al. Tumor-associated lymphatic vessel density is a postoperative prognostic biomarker of hepatobiliary cancers: a systematic review and meta-analysis. *Front Immunol*. 2024;15:1519999. doi:10.3389/fimmu.2024.1519999
21. Morse MA, Sun W, Kim R, et al. The role of angiogenesis in hepatocellular carcinoma. *Clin Cancer Res*. 2019;25(3):912–920. doi:10.1158/1078-0432.CCR-18-1254
22. Ishigami K, Yoshimitsu K, Nishihara Y, et al. Hepatocellular carcinoma with a pseudocapsule on gadolinium-enhanced MR images: correlation with histopathologic findings. *Radiology*. 2009;250(2):435–443. doi:10.1148/radiol.2501071702
23. An C, Rhee H, Han K, et al. Added value of smooth hypointense rim in the hepatobiliary phase of gadoxetic acid-enhanced MRI in identifying tumour capsule and diagnosing hepatocellular carcinoma. *Eur Radiol*. 2017;27(6):2610–2618. doi:10.1007/s00330-016-4634-6
24. Rhee H, An C, Kim HY, Yoo JE, Park YN, Kim MJ. Hepatocellular carcinoma with irregular rim-like arterial phase hyperenhancement: more aggressive pathologic features. *Liver Cancer*. 2019;8(1):24–40. doi:10.1159/000488540
25. Hong SB, Choi SH, Kim SY, et al. MRI features for predicting microvascular invasion of hepatocellular carcinoma: a systematic review and meta-analysis. *Liver Cancer*. 2021;10(2):94–106. doi:10.1159/000513704
26. Au KY, Chan KKS, Lo RCL. A clinicopathological study of young-onset hepatocellular carcinoma. *Anticancer Res*. 2021;41(6):2933–2944. doi:10.21873/anticanres.15075
27. Yan Q, Sun YS, An R, et al. Application and progress of the detection technologies in hepatocellular carcinoma. *Genes Dis*. 2023;10(5):1857–1869. doi:10.1016/j.gendis.2022.04.003
28. Wei H, Jiang H, Zheng T, et al. LI-RADS category 5 hepatocellular carcinoma: preoperative gadoxetic acid–enhanced MRI for early recurrence risk stratification after curative resection. *Eur Radiol*. 2021;31(4):2289–2302. doi:10.1007/s00330-020-07303-9
29. Bagheri Lankarani K, Honarvar B, Seif MA, et al. Outcome of liver transplant patients with intraoperative-detected portal vein thrombosis: a retrospective cohort study in Shiraz, Iran. *Exp Clin Transplant*. 2021;19(4):324–330. doi:10.6002/ect.2018.0295